




Research Article

Bemotrizinol-Loaded Carnauba Wax-Based Nanostructured Lipid Carriers for Sunscreen: Optimization, Characterization, and *In vitro* Evaluation

Thayse S. Medeiros,^{1,2} Lívia M. C. C. Moreira,² Tiago M. T. Oliveira,² Demis F. Melo,^{1,2} Eduardo P. Azevedo,³ Amanda E. G. Gadelha,⁴ Marcus V. L. Fook,⁴ João A. Oshiro-Júnior,^{1,5} and Bolívar P. G. L. Damasceno^{1,2,5} 

Received 11 February 2020; accepted 15 September 2020; published online 18 October 2020

Abstract. Nanostructured lipid carriers (NLC) are aqueous dispersions of nanoparticles formed by solid and liquid lipids. In this study, NLC containing an organic UV filter, bemotrizinol, were developed for sunscreen formulation using carnauba wax and caprylic/capric triglycerides through ultrasonication technique. A Box-Behnken design was used to evaluate the influence of three variables on the particle size with the purpose of choosing the best system for further characterization. The particle size decreased as the surfactant concentration increased, reaching an average size of 122.4 ± 0.3 nm at 30 days of storage. Scanning electron microscopy showed intact and spherical particles. Thermal analysis and Fourier-transform infrared spectroscopy suggest that bemotrizinol was incorporated into the NLC. The X-ray diffraction showed a reduction in the crystallinity of the NLC. *In vitro* analysis indicated an improvement in the photoprotective activity of bemotrizinol when incorporated into NLC. These findings suggest a promising, stable, and biocompatible system.

KEY WORDS: lipid nanoparticles; nanotechnology; nanostructured lipid carriers; UV filters; photoprotection; sunscreens; Box-Behnken design.

INTRODUCTION

The sun, a great source of natural energy, is essential for human health as it is involved in several chemical, biochemical, and metabolic processes such as vitamin D photosynthesis. However, such activities depend on the intensity of exposure to the ultraviolet (UV) radiation (1,2).

UV radiation is part of the electromagnetic spectrum which is subdivided into three subtypes of radiation: UVA (320 to 400 nm), UVB (280 to 320 nm), and UVC (100 to

280 nm). UVC radiation is completely absorbed by the ozone layer, whereas UVB accounts for 5% of the UV radiation that reaches the earth's surface. The other 95% corresponds to UVA (2–4).

UVA radiation reaches the deepest layers of the skin through the epidermal junctions where melanocytes reside and are primarily responsible for the early aging (5). On the other hand, UVB radiation reaches the superficial layers of the skin, whose exacerbated exposure confers sunburn, which is characterized by erythema, edema, and pain. In addition, both UVA and UVB radiations interact with the human DNA, which results in cross-linkage of the pyrimidine bases. If the dimers of the damaged DNA are not repaired, it can lead to mutations that might result in skin cancer (6,7).

In order to minimize and prevent inconveniences related to exposure to UV radiation, several studies have been conducted to develop photoprotectors that are more stable and safer (8). Photoprotectors are classified as inorganic and organic filters. Inorganic filters are minerals that act by reflecting or scattering radiation. Organic filters, however, absorb the radiation and dissipate it in the form of heat (1,9,10).

The safety of sunscreens is mainly related to their effects on the skin (irritation and sensitization) and also to the possibility of skin permeation and accumulation in the body, which can generate systemic side effects such as phototoxic and photoallergic reactions (7). In addition, they may present

Electronic supplementary material The online version of this article (<https://doi.org/10.1208/s12249-020-01821-x>) contains supplementary material, which is available to authorized users.

¹ Graduation Program in Pharmaceutical Sciences, Center for Biological and Health Sciences, Department of Pharmacy, State University of Paraíba (UEPB), Av. Juvêncio Arruda, s/n, Bairro Universitário, Campina Grande, PB 58429-600, Brazil.

² Laboratory of Development and Characterization of Pharmaceutical Products, Department of Pharmacy, State University of Paraíba, Campina Grande, PB, Brazil.

³ Graduate Program of Biotechnology, Laureate International Universities - Potiguar University, Natal, RN, Brazil.

⁴ Laboratory of Biomaterials Evaluation and Development of the Northeast, Federal University of Campina Grande, Campina Grande, PB, Brazil.

⁵ To whom correspondence should be addressed. (e-mail: joaoshiro@yahoo.com.br; bolivarpd@servidor.uepb.edu.br)

instability that can trigger photochemical reactions that compromise their physical properties as well as their photoprotective efficacy (10–13).

Due to these limitations, nanosystems have been developed for photoprotection (14–23). Thus, an attractive strategy is the use of nanostructured lipid carriers (NLC) which are aqueous dispersions of nanoparticles formed by mixtures of solid and liquid lipids (24,25). NLC are well tolerated by the human body and compatible with large numbers of molecules, have physical and chemical stability, and provide greater encapsulation efficiency (26,27).

In addition, NLC have demonstrated potential for topical application due to their adhesiveness as they form a film over the skin, providing an occlusive effect (27,28). Besides, they are suitable systems for the incorporation of photoprotective agents such as organic filters. Once these agents are incorporated into the lipid matrix, their release can be controlled and prolonged. In addition, this incorporation may improve the stability of the sunscreen as it will be less susceptible for photochemical reactions. Some solid lipids used for obtaining NLC also act as physical filters, providing a synergistic effect and consequently reducing the amount of sunscreen necessary to achieve the optimum photoprotective effect (16,29).

Villalobos-Hernández and Müller-Goymann (2006) obtained an increase in the sun protection factor (SPF) when incorporating TiO₂ to NLS. Likewise, Puglia *et al.* and Nikolic *et al.* developed NLC containing a mixture of organic sunscreens and obtained SPF higher than those found in conventional sunscreens, relating this fact to the synergism existing between the solid lipid used in the development of these nanocarriers and the sunscreen itself (15,16,18).

Thus, the strategy of incorporating a sunscreen to NLC has numerous advantages, such as better stability of the sunscreen, maintaining the sunscreen on the skin for a longer time, as well as higher photoprotective effect and less esthetic inconveniences, such as the oiliness that is usually generated by conventional sunscreens.

In this context, the aim of this study was to develop, optimize, and characterize NLC containing bemotrizinol (bis-ethylhexyloxyphenol methoxyphenyl triazine), an organic UV filter with a broad absorption spectrum that covers wavelengths from 280 to 380 nm (UVA and UVB) (30), commercially known as Tinosorb[®] S, using an experimental design Box-Behnken type.

MATERIAL AND METHODS

Material

Bemotrizinol (bis-ethylhexyloxyphenol methoxyphenyl triazine, Basf, Ludwigshafen am Rhein, Germany) was used as the organic filter. Polysorbate 80 (All Chemistry, Sao Paulo, Brazil) and Span[®] 80 (sorbitan monooleate, Sigma-Aldrich, St. Louis, USA) were the two non-ionic surfactants used to stabilize the formulation. Carnauba wax (All Chemistry, São Paulo, Brazil) and caprylic/capric triglycerides (All Chemistry, São Paulo, Brazil) were used as the solid and liquid lipids, respectively. The aqueous phase of all formulations was distilled water.

Methods

Experimental Design

By using the software Statistica 10 (StatSoft), the formulation was optimized by carrying out an experimental design of Box-Behnken type with three factors and three levels each (high, medium, and low), as shown in Table I. Bemotrizinol (BEMT) concentration (X1), surfactant concentration (X2), and sonication time (X3) were considered independent variables, whereas particle size (Y) was the dependent variable (response). The experimental matrix consisted of twelve runs and four central points, being three replications, which yielded a total of 16 formulations.

Preparation of the NLC

The blank nanostructured lipid carriers (NLCB) and nanostructured lipid carriers with BEMT (NLCF) were developed using the cavitation shaking technique with an ultrasonic cell disruptor (Unique, Indaiatuba, SP, Brazil) for particle fragmentation. Carnauba wax (0.2 g) and caprylic/capric triglycerides (0.05 g), representing 5% of the formulation, polysorbate 80 and Span[®] 80 (0.15 g and 0.04 g, respectively), and bemotrizinol (0.02 g) were heated together at about 10°C above the melting temperature of carnauba wax (CC) (approximately 80°C). The aqueous phase (distilled water) was heated to the same temperature and poured into the oily phase followed by sonication for two cycles of 7 min each at 200 W. Finally, the vials were placed in an ice bath for cooling and solidification of the particles.

Particle Size and Zeta Potential Analyses

Particle size and zeta potential were determined by dynamic light scattering (DLS) technique and by measuring the electrophoretic mobility of suspended particles using a Zetasizer Nano equipment (Malvern, Montgomeryville, USA). Samples were diluted in distilled water following the proportion of 1:100 (v/v), and the readings were taken at 1, 7, 15, and 30 days. For the zeta potential, the measurements were repeated three times at 25°C with a field strength of 20 V/cm. Samples were diluted at 1:100 (v/v) in distilled water and the readings were taken at 1, 7, 15, and 30 days.

Table I. Factors and Levels for Box-Behnken Design 3³

Factors	Code levels		
	-1	0	1
X1	0.3	0.4	0.5
X2	2	3	4
X3	3	5	7

X1, UV filter concentration (%) (FC); X2, surfactant concentration (%) (SC); X3, sonication time (min) (T)

Morphological Analysis by Scanning Electron Microscopy

The morphology of the particles was evaluated through a high-resolution scanning electron microscope (SEM-FEG), model JSM-7500F (JEOL, Boston, USA). After diluting each sample in distilled water 1:30 (v/v), one drop was placed on a metal support followed by drying at room temperature for 3 days in a desiccator. The dried material was then coated with conductive carbon, and the photomicrographs were obtained under 50,000 of magnification.

Differential Scanning Calorimetry Analysis

The differential scanning calorimetry (DSC) curves was performed with each individual component of the formulation, as well as with the lyophilized systems and binary mixtures (1:1) of bemotrizinol with each of the other components. Four milligrams of each sample was weighted and sealed in aluminum crucibles. DSC curves were obtained using a calorimeter module Q20 (TA Instruments, New Castle, DE, USA) at a temperature range of 20 to 300°C, with a heating rate of 10°C/min under a nitrogen flow of 50 mL/min.

Thermogravimetric Analysis

The thermogravimetric (TG) curves for each individual component as well as the lyophilized systems were obtained using the simultaneous TG tester model SDT Q600 (TA Instruments, New Castle, DE, USA) under nitrogen flow of 100 mL/min, heating rate of 10°C/min, and temperature range of 25–900°C, using 4 mg of sample previously weighed in alumina crucible.

X-ray Diffraction Analysis

The data were obtained using a XRD 7000 diffractometer (Shimadzu, Kyoto, Japan), with open angle of 2θ within the range of 5–60°, system θ-θ, using Cu radiation (λ = 1.5418 Å), at a step of 0.02° (θ) and 1.0 s of interval for each sample.

Fourier-Transform Infrared Spectroscopy

Fourier-transform infrared spectroscopy with attenuated total reflectance (FTIR-ATR) was performed in the wave-number range of 4000–600 cm⁻¹ using a Spectrum 400 equipment (Perkin Elmer, Waltham, MA, USA).

In vitro Photoprotective Activity

The absorbance spectra of NLCF and a solution of bemotrizinol in ethyl alcohol of equal concentrations (4% of BEMT in 5 mL of solution) were obtained at wavelengths of 290 to 400 nm using a UV-1900 UV-Vis spectrophotometer (Shimadzu, Kyoto, Japan). Both the nanosystem and the BEMT solution were diluted in distilled ethyl alcohol at a ratio of 1:500 (v/v).

In vitro Determination of the Sun Protection Factor

The *in vitro* determination of SPF was performed following the method described by Mansur *et al.* (31) using a UV-Vis spectrophotometer 12-40 (Shimadzu, Kyoto, Japan). The SPF was determined for NLCF, NLCB, and bemotrizinol solution in isopropyl alcohol at the same concentration (4% of BEMT in 5 mL of solution) of the filter-loaded nanosystem and a commercially available sunscreen (Sundown[®] SPF 30).

After the formulations were diluted in isopropyl alcohol to the final concentration of 0.2 mg/mL, the absorbances were determined in the range of 290 to 320 nm with intervals of 5 nm. The experiment was performed in triplicate for each wavelength. The SPF was calculated using Eq. 1:

$$\text{SPF}_{\text{spectrophotometric}} = CF : \sum_{290}^{320} EE(\lambda) \cdot I \cdot \text{Abs}(\lambda) \quad (1)$$

where SPF is the sun protection factor; *CF* is the correction factor (=10), determined according to two sunscreens at known SPF such that a cream containing 8% of homosalate resulted in a SPF of 4; *EE* is the erythemogenic effect of wavelength radiation (λ); *I* is the intensity of sunlight at a corresponding wavelength (λ); and *Abs* (λ) corresponds to the absorbance of the formulation solution containing the sunscreen at wavelength (λ). The values of *EE* (λ) and *I* (λ) (Table II) were previously determined (32).

Equation 2 was used to calculate the corrected value of SPF based on the commercially available sunscreen (PC):

$$\text{SPF}_{\text{corrected}} = \frac{\text{SPF}_{\text{spectrophotometric}} \times \text{SPF}_{\text{labeled}}}{\text{SPF}_{\text{pc}}} \quad (2)$$

where $\text{SPF}_{\text{spectrophotometric}}$ is the spectrophotometric value obtained for each formulation following the method of Mansur *et al.* (31), $\text{SPF}_{\text{labeled}}$ is the value expressed on the label of the commercially available sunscreen, and SPF_{pc} is the value obtained of the commercially available sunscreens using the reported method.

RESULTS AND DISCUSSION

Box-Behnken Experimental Planning for NLC Development

In order to obtain particle sizes below 200 nm, an experimental design was conducted. The particle sizes of the 16 formulations varied between 149 nm (NLC4) and 470 nm

Table II. Relationship Between Erythemogenic Effect (EE) and Intensity of Radiation (I) for Each Wavelength

λ (nm)	EE × I
290	0.0150
295	0.0817
300	0.2874
305	0.3278
310	0.1864
315	0.0839
320	0.0180
Σ	1.0000

(NLC9), depending on the values of the independent variables (Table III). The results of the statistical analysis (ANOVA—analysis of variance) show the effects and levels of significance of the variables on the particle size (Table IV).

The concentration of surfactant was the variable that had the highest level of significance, which corroborates the findings of Pardeike *et al.* (24) who showed that the higher the concentration of surfactants, the smaller the size of the obtained particles. This can be explained by the steric hindrance created on the surface of the particles by the surfactant, which prevented the coalescence and aggregation of smaller to larger particles, thereby increasing the stability of smaller carriers (33).

Figure 1 shows the response surface and how the dependent variable (size) reacts to different levels of each independent variable.

It was observed that the lower the surfactant concentration, the larger the particle size. The response surfaces show that the surfactant concentration variable remains unchanged, which means that the particle size might be smaller at higher surfactant concentrations without being influenced by stirring time or BEMT concentration (Fig. 1a and b).

The interaction between the variables *T* and *FC* is significant ($p < 0.05$) (Fig. 1c), whereas the concentration of BEMT influences the stirring time.

The line that is depicted in the figure of predicted values *versus* observed values (Fig. A.1) represents the equation of the mathematical model, and the points are the results of the experimental design. The closer to the line is, the more acceptable the model will be. Of the 16 formulations, four results were left out of the line and, therefore, it can be inferred that this model is considered acceptable.

In addition, if the model is well adjusted, the lack of fit will have the same intensity as random errors, which means that for a model to be considered acceptable, the lack of fit will not be significant ($p > 0.05$). These results are shown in Table V.

Table III. Box-Behnken Planning Matrix and Response

Formulation	X1 FC (%)	X2 SC (%)	X3 T (min)	Response Size (nm)
1	0.3	2	5	429.90
2	0.5	2	5	419.50
3	0.3	4	5	196.50
4	0.5	4	5	149.00
5	0.3	3	3	214.40
6	0.5	3	3	384.20
7	0.3	3	7	282.10
8	0.5	3	7	338.40
9	0.4	2	3	470.00
10	0.4	4	3	308.00
11	0.4	2	7	335.10
12	0.4	4	7	149.90
13	0.4	3	5	170.40
14	0.4	3	5	204.10
15	0.4	3	5	164.70
16	0.4	3	5	236.20

FC UV filter concentration, SC surfactant concentration

Table IV. Analysis of Variance (ANOVA) of the Quadratic Model for the Response Size

Factor	SS	df	MS	F-value	p value
CF (L)	3536.6	1	3536.4	3.21666	0.170179
CF (Q)	8817.2	1	8817.2	8.02000	0.066083
CT (L)	90,546.4	1	90,546.4	82.35958	0.002826
CT (Q)	13,421.2	1	13,421.2	12.20773	0.039653
T (L)	9186.9	1	9186.9	8.35626	0.062976
T (Q)	16,371.2	1	16,371.2	14.89099	0.030756
Lack of fit	29,245.8	6	4874.3	4.43359	0.124607
Pure error	3298.2	3	1099.4		
Total SS	174,423.4	15			

SS sum of squares, df degrees of freedom, MS mean square

Thus, the nanocarriers with the lowest mean particle size were NLC4 and NLC12 with sizes of 149 and 149.9 nm, respectively. Due to their similar average sizes, the criterion for choosing the ideal system was the particle size distribution, with NLC12 being chosen for further analysis.

Particle Size Analysis, Polydispersity Index, and Zeta Potential

According to the results of the experimental design, the NLC12 formulation was chosen for the incorporation of the organic filter and for further evaluation of the stability during storage, which was performed through determination of the average particle size, polydispersity index (PDI), and zeta potential, as shown in Fig. 2 and Table V.

The results show that the sizes of the nanosystems without (NLCB) and with the organic filter (NLCF) after 24 h were 117.2 ± 0.2 nm and 122.4 ± 0.2 nm, respectively. After 30 days of storage, the sizes were 117.3 ± 0.4 nm and 122.4 ± 0.3 nm, respectively. However, no statistical differences were observed on the particle sizes between the 7th and 15th days of storage, which seems to indicate that there was no aggregation of the particles. The particle sizes of both systems were in accordance with other previous reports (18,34–36).

The PDI values were less than 0.18 for both NLCB and NLCF during 30 days of storage, which indicates a narrow and uniform size distribution (37,38).

According to Jain *et al.* (27), the topical application of NLC results in a thin layer of film over the skin, causing an occlusive effect, which might contribute to the maintenance of skin hydration and a longer residence time in the area of application. These properties are related to particle size. In fact, Wissing *et al.* (39) revealed that particles smaller than 400 nm exhibit better adhesion properties when compared with larger ones.

Such effect may favor the retention of these NLC in the stratum corneum and epidermis, therefore preventing the molecule from permeating the deep layers of the skin and reaching the systemic circulation. This hypothesis is supported by previous reports that have shown the lack or minimum skin permeation of molecules when incorporated into these lipid nanocarriers (40–42).

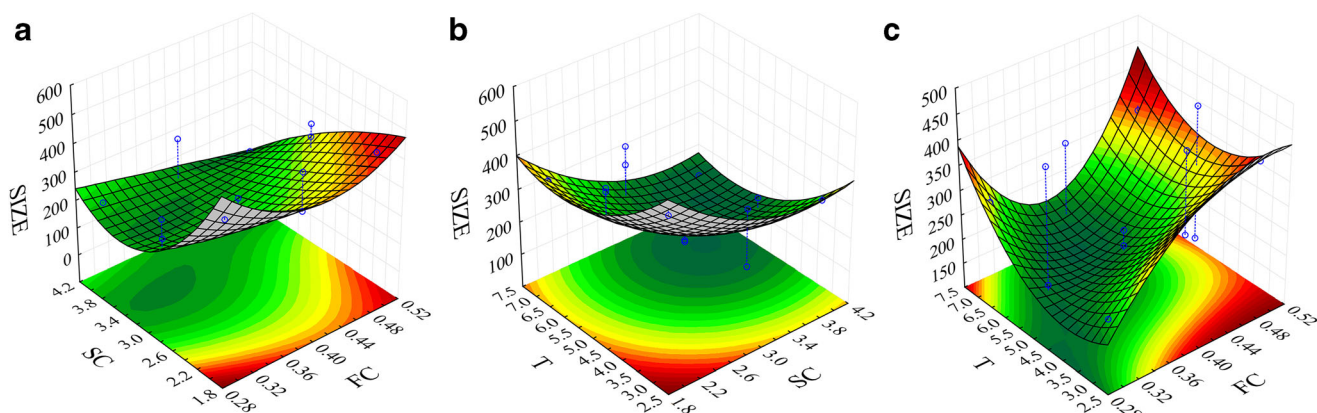


Fig. 1. 3D response surface of the correlation between: **a** BEMT concentration (FC) and surfactant concentration (SC); **b** sonication time (T) and surfactant concentration (SC); **c** sonication time (T) and BEMT concentration (FC)

Pinto and collaborators (43), for instance, evaluated topical distribution of NLC loaded with α -tocopherol and fluorescence marker after administration in a 3D model of reconstituted human epidermis, where they found that most of the nanocarriers were retained in the stratum corneum.

In addition, Haque *et al.* (44) evaluated the permeation profile of three organic UV filters, including BEMT, and found that no permeation occurred towards the deeper layers of the skin. Similar result was found by Puglia *et al.* (18) when incorporating BEMT into NLC. Therefore, based on these findings, it seems likely to infer that similar results are expected for NLCB and NLCF.

The zeta potential analysis revealed that the surface charges of the particles were -19.2 ± 0.17 mV and -19.3 ± 0.42 mV for NLCB and NLCF, respectively. Villalobos-Hernández and Müller-Goymann (15) obtained similar results for NLC using carnauba wax and decil oleate, respectively. According to these authors, the zeta potential increased as the percentage of carnauba wax increased in the formulation, suggesting that the amount of wax may influence the stability of the formulations. In fact, for particles that received steric stabilization with the use of surfactants, values of $|20|$ mV are sufficient to guarantee long-term stability, suggesting minimal predisposition for long-term aggregation (28).

Morphological Analysis by Scanning Electron Microscopy

The morphology of the nanoparticles was analyzed by scanning electron microscopy (SEM), as shown in Fig. 3. The

NLCB and NLCF (Fig. 3a and b, respectively) were intact and spherical. The particle sizes corroborate with those obtained by DLS, and the photomicrographs show the absence of any sort of aggregation.

Differential Scanning Calorimetric Analysis

DSC curves for each individual component as well as the lyophilized NLCB and NLCF are shown in Fig. 4a. The curves for the binary mixtures (1:1) between each component and bemotrizinol are shown in Fig. 4b.

The DSC curve for CW (Fig. 4a) shows two endothermic events, the first at 59.52°C (Table V) and the second at 78.34°C , where both are related to its melting. BEMT showed an endothermic peak at 82.53°C , which is in accordance with the manufacturer's data (BASF).

In order to investigate any sort of interaction between BEMT and the other components of the formulation, 1:1 binary mixtures of BEMT with each individual component were prepared, whose DSC curves are shown in Fig. 4b. In the mixture of BEMT and CW, two endothermic peaks of similar energies are observed at 57.04°C and 78.36°C (Table VI), which correspond to the melting of carnauba wax and bemotrizinol, respectively. However, a decrease in the melting temperature was observed in the DSC curve for the binary mixture of BEMT and CCT, which seems to be due to the dissolution of BEMT within the CCT matrix as a result of hydrophobic interactions. Both events may induce a disorder in the crystalline structure of BEMT (45). On the

Table V. Particle Size, Zeta Potential (ZP), and Polydispersity Index (PDI) Values According to the Storage Time (Mean \pm Standard Deviation; $n = 3$) of Blank Nanostructured Lipid Carriers (NLCB) and Nanostructured Lipid Carriers with Organic UV Filter (NLCF)

NLCB				NLCF		
Day	Size (nm)	ZP (mV)	PDI	Size (nm)	ZP (mV)	PDI
1st	117.2 ± 0.2	-28.8 ± 0.5	0.16 ± 0.0	122.4 ± 0.2	-28.7 ± 0.9	0.14 ± 0.0
7th	120.6 ± 0.8	-21.6 ± 1.2	0.14 ± 0.0	123.5 ± 0.9	-21.8 ± 0.2	0.13 ± 0.0
15th	118.8 ± 0.7	-19.3 ± 0.3	0.17 ± 0.0	123.6 ± 0.1	-19.8 ± 0.4	0.13 ± 0.0
30th	117.3 ± 0.4	-19.2 ± 0.2	0.16 ± 0.0	122.4 ± 0.3	-19.3 ± 0.4	0.13 ± 0.0

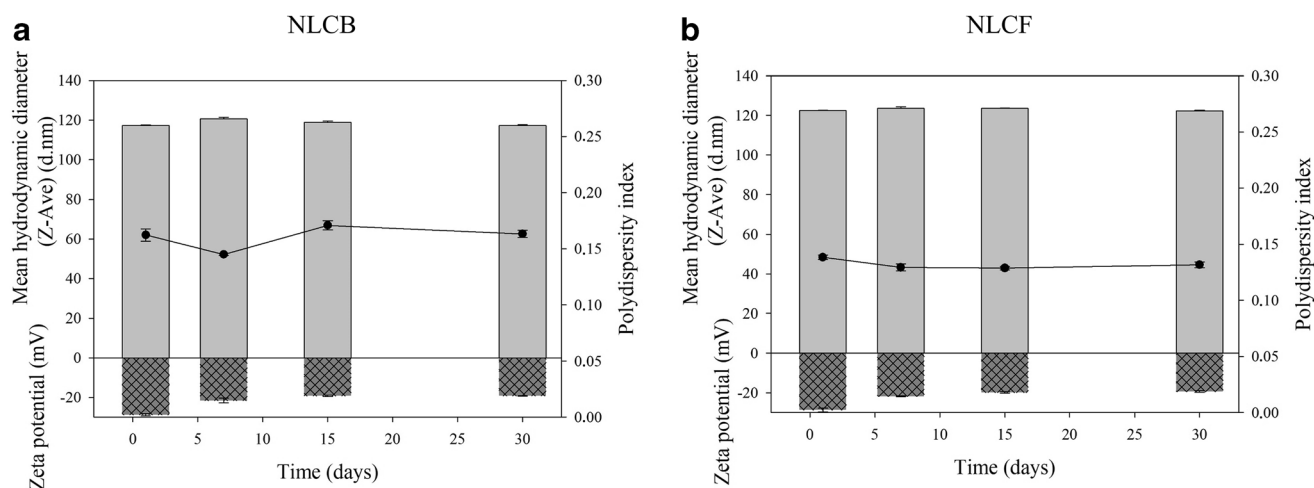


Fig. 2. Determination of the mean hydrodynamic diameter (Z-Ave) (d.nm), polydispersity index, and zeta potential according to the storage time (mean \pm standard deviation; $n = 3$) of blank nanostructured lipid carriers (NLCB) and nanostructured lipid carriers with organic UV filter (NLCF)

other hand, no significant changes were observed in the endothermic events of the other binary mixtures.

NLCB presented endothermic events similar to that of NLCF. The DSC curve for NLCF shows two endothermic events at 58.68°C and 76.99°C, which confirms the integrity of the carnauba wax, suggesting that there were no changes in its original structure. On the other hand, the endothermic events related to BEMT are not present in the DSC curve for NLCF. Previous reports have shown that when the endothermic events of the encapsulated material disappear, it might be an indication that its crystallinity has been reduced. In addition, it might indicate that BEMT has been homogeneously dispersed within the nanocarrier matrix (46).

Thermogravimetric Analysis

Figure 5 shows the results obtained for the thermogravimetric analysis.

The thermal decomposition of NLCB and NLCF occurred at 131 and 139°C, respectively, which differ from that of the major component, CW (146°C). Such a difference

seems to be related to the reduction of crystallinity of CW when the liquid lipid (CCT) is added to the formulation. By analyzing the decomposition temperatures of the NLC, one can infer that the incorporation of BEMT to the lipid nucleus resulted in new chemical interactions (hydrophobic/hydrophobic), which might have increased the energy requirement for its decomposition (Table VII).

However, at temperatures above the melting point of CW (>59.52°C), BEMT melts and exhibits a slight loss of mass during the further heating process. TG thermograms (Fig. 5) show that no loss of BEMT mass occurs up to 300°C. In this current study, the nanocarrier systems were obtained by heating (80°C) up above the melting temperature of the lipid phase. Thus, the results indicate that decomposition of bemotrizinol during the nanoparticle production can be ruled out due to its high thermal stability.

X-ray Diffraction Analysis

The XRD analyses were performed with the purpose of evaluating the changes in crystallinity of the main compo-

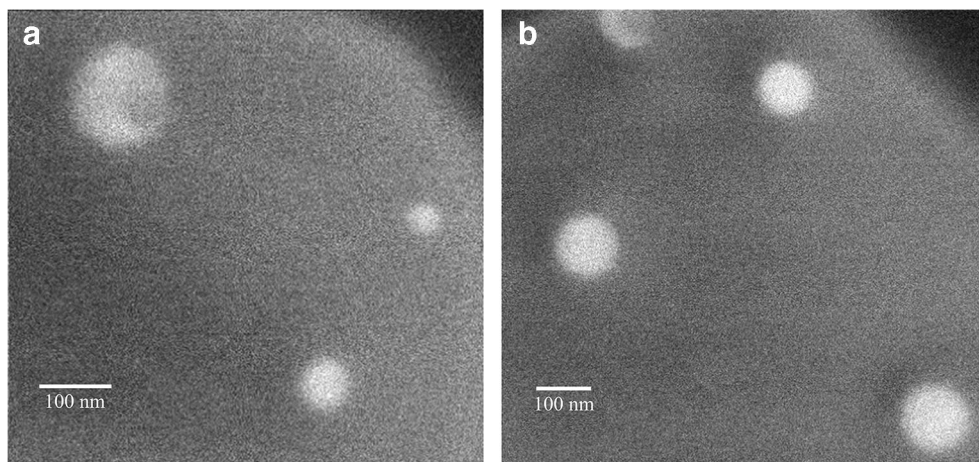


Fig. 3. Two-dimensional photomicrographs of NLCB (a) and NLCF (b)

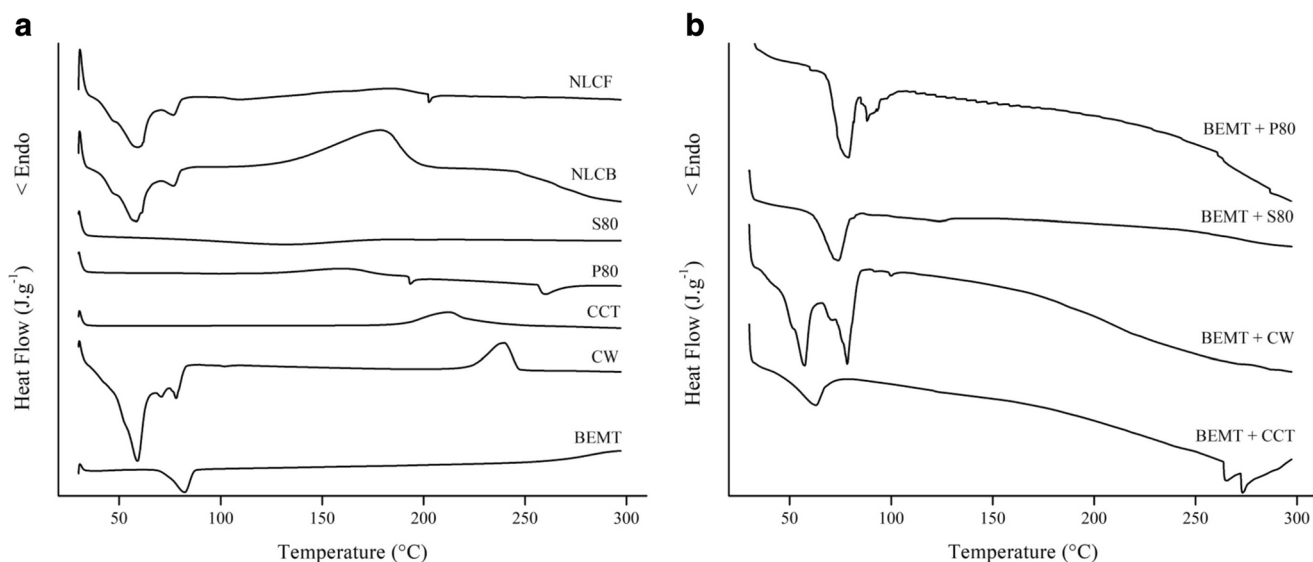


Fig. 4. DSC curves for NLCB, NLCF, individual components Span[®] 80 (S80), polissorbate 80 (P80), caprylic/capric triglycerides (CCT), carnauba wax (CW), bemotrizinol (BEMT), and physical mixtures (1:1) of BEMT + P80, BEMT + S80, BEMT + CW, and BEMT + CCT

nents of the formulation, as well as investigating the influence of the presence of liquid lipid in the crystallinity. The diffractograms of solid lipid (carnauba wax), bemotrizinol, and the nanosystems without and with bemotrizinol are shown in Fig. 6.

The diffractogram of carnauba wax (a) presented several diffraction peaks, where those at 21° and 24° (angles dispersed at 2 θ) are the most intense ones, therefore

Table VI. DSC Data for NLCB, NLCF, Excipients, and Their Respective Binary Mixtures

Sample	Event	Peak (°C)	ΔH (J g ⁻¹)
BEMT	First	82.53	17.17
CW	First	59.52	47.17
	Second	78.34	5.09
	Third	239.84	31.89
BEMT + CCT (1:1)	First	57.04	35.93
	Second	78.36	33.44
S80	First	131.75	24.67
BEMT + S80 (1:1)	First	74.01	20.59
P80	First	193.47	1.85
	Second	259.78	6.77
BEMT + P80 (1:1)	First	78.93	25.67
	Second	88.12	3.95
CCT	First	212.41	30.80
BEMT + CCT (1:1)	First	62.96	15.93
NLCB	First	58.25	56.73
	Second	77.06	4.81
	Third	178.74	127.4
NLCF	First	58.68	53.76
	Second	76.99	3.66
	Third	202.60	1.42

BEMT bemotrizinol, CW carnauba wax, S80 Span[®] 80, P80 polissorbate 80, CCT caprylic/capric triglycerides, NLCB blank nanostructured lipid carriers, NLCF nanostructured lipid carriers with organic UV filter

corroborating the crystalline nature of the solid lipid used in this current study as previously described by Freitas *et al.* (47). Bemotrizinol (b) presented several diffraction peaks with those at 7°, 13°, 24°, and 29° being the most intense ones, which also confirms its crystalline nature.

Both carnauba wax and BEMT partially lost their crystalline nature when incorporated into the NLC. The diffractograms of NLC show an enlargement at the beginning of the peak around 21°, which seems to be due to the presence of CCT in the formulation, resulting in the appearance of amorphous halos, therefore interfering in the organization of its crystalline structure.

The change in the BEMT's diffraction pattern seems to be due to a crystalline-to-amorphous transition, which is a known phenomenon that usually results in increased solubility (48). This finding is supported by the DSC data (Fig. 4a), which showed that BEMT endothermic peak disappeared only in the DSC curve for NLCF but not in those for the physical mixtures. This suggests its homogeneous dispersion within the lipid matrix (41,49).

Sanad *et al.* (50) developed NLC containing oxybenzone using CCT and oleic acid as liquid lipids in which they observed that a significantly higher entrapment efficiency was achieved with CCT. Since it is a mixture of triglycerides of different chain lengths, crystals with many imperfections are a common feature of CCT, which seems to offer more space to accommodate molecules of varying sizes.

Previous reports have found that the addition of liquid lipids to lipid matrix, with its consequent reduction in crystallinity, increases the entrapment capacity of these matrices (43,51–53), which might explain the high entrapment efficiency of BEMT into the NLCF.

Furthermore, the release behavior of molecules incorporated into NLC can be influenced by different factors, such as the type of solid lipid used, the proportion between lipids, the type and concentration of stabilizer, the temperature used, and the particle size (28,54–55).

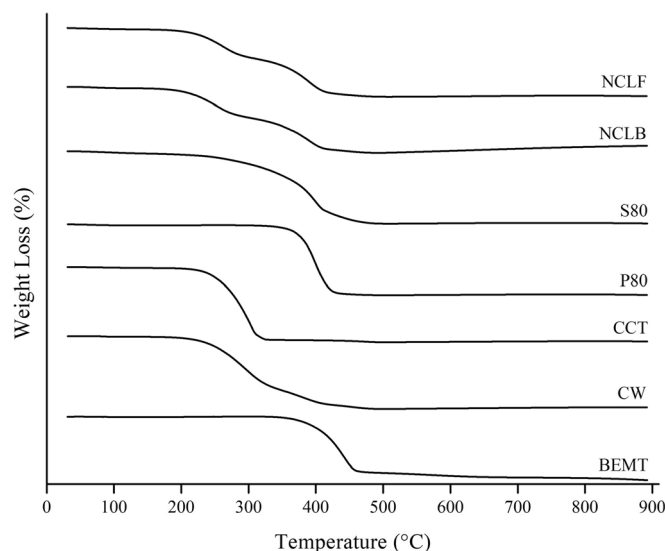


Fig. 5. TG curves for NLCB, NLCF, and each individual component Span[®] 80 (S80), polissorbate 80 (P80), caprylic/capric triglycerides (CCT), carnauba wax (CW), and bemotrizinol (BEMT)

However, several authors report a biphasic release profile of molecules from NLC, with a rapid initial release followed by a more sustained pattern (53,56–58). This might be explained by the fact that the release of molecules is controlled by two mechanisms: diffusion through the matrix, which depends on the dissolution of the molecule in the aqueous medium, and erosion of the lipid matrix, which is determined by the rate of lipid degradation (55,59).

Octyl p-methoxycinnamate (60) and oxybenzone (50) have been incorporated into NLC, in which a biphasic release profile was observed in both studies. Thus, the same profile is expected for NLCF, with the BEMT fraction adhered to the

NLCF surface being released more quickly and the fraction entrapped in the lipid matrix being released slowly.

Fourier-Transform Infrared Spectroscopy

The purpose of the FTIR-ATR analysis was to investigate the occurrence of chemical interactions between the components of the formulations. The FTIR spectra of the individual components as well as the NLCB and NLCF formulations are shown in Fig. 7.

The spectrum of bemotrizinol (Fig. 7) shows peaks in the 1550–850 cm^{-1} region which have been attributed to the C–C stretch of carbon-carbon bond and C–O–C of ether. The peak at 1570 cm^{-1} refers to C=N bond of the triazine group of BEMT. The peaks in the 2000–2600 cm^{-1} region refer to C=C=C from the benzene rings. In addition, the peaks in the 2500–4000 cm^{-1} are attributed to the –OH stretch of the hydroxyl groups and –CH of the alkane groups.

The spectra of NLCB and NLCF show a predominance of peaks related to the surfactants and lipids, especially those attributed to carnauba wax. What differentiates the NLCB spectrum from that of NLCF is the additional bands at 1550 to 1650 cm^{-1} in the latter, which corresponds to the C=N bonds found only in bemotrizinol as indicated in Fig. 7. Since the concentration of bemotrizinol is lower than those of the other components, its characteristic bands appear at lower intensity when compared with the bands attributed to the other components. In addition, the subtle appearance of BEMT bands in the NLCF spectrum seems to indicate that it was incorporated into the nanocarrier. Similar findings were observed in the study conducted by Tahir *et al.* (61).

Table VII. TG Data for BEMT, NLCB, NLCF, and the Other Components

Sample	Stage	Start–end (°C)	Weight loss (%)
CW	First	146.32–253.31	72.34
	Second	253.31–432.11	19.04
	Third	432.11–512.82	4.63
BEMT	First	308.68–498.58	74.75
S80	First	30.00–220.38	5.42
	Second	220.38–419.77	76.15
	Third	419.77–516.62	14.78
P80	First	276.40–518.51	92.80
CCT	First	171.01–343.81	95.28
	Second	343.81–508.07	2.38
NLCB	First	131.13–304.88	39.52
	Second	304.88–430.21	42.44
	Third	430.21–507.12	3.46
NLCF	First	139.68–317.23	40.27
	Second	317.23–515.67	49.42

BEMT bemotrizinol, CW carnauba wax, S80 Span[®] 80, P80 polissorbate 80, CCT caprylic/capric triglycerides, NLCB blank nanostructured lipid carriers, NLCF nanostructured lipid carriers with organic UV filter

In vitro Evaluation of Photoprotective Potential and Spectrophotometric SPF

A UV-Vis spectrophotometric scan allows a qualitative analysis of the potential photoprotective effect of the

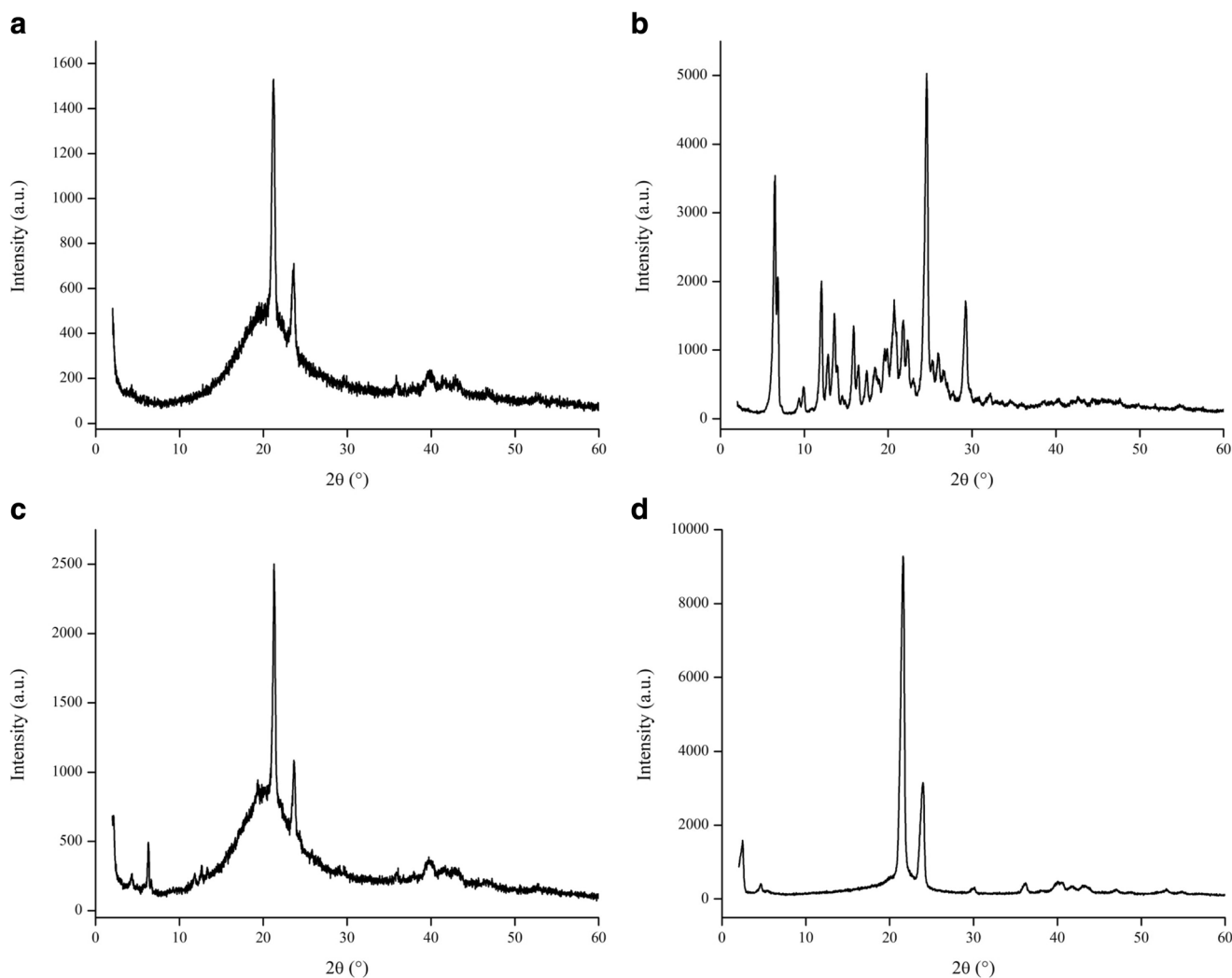


Fig. 6. Diffractograms of carnauba wax (a), BEMT (b), NLCB (c), and NLCF (d)

bemotrizinol incorporated into the nanosystem in comparison with that of bemotrizinol alone (Fig. 8).

Figure 8 shows that a marked increase in the absorbance was observed when bemotrizinol was incorporated into the nanocarriers, especially in the range of 290–380 nm. It is possible to observe that the difference between the absorbances of the BEMT solution (b) and the NLCF (a) is similar to the absorbance of the system without BEMT (NLCB) (c), which seems to prove the synergistic effect between BEMT and the solid lipid (carnauba wax). These findings corroborate that of Nikolic *et al.* (16) when they determined the absorbances of different nanostructured lipid carriers containing the same type and concentration of organic filter, changing only the lipid, where a higher absorbance was observed with the samples prepared with carnauba wax. In fact, Villalobos-Hernández and Müller-Goymann (62) had previously reported that carnauba wax has an intrinsic property of filtering UV radiation.

The *in vitro* spectrophotometric method in the UVB region was used to quantitatively determine the SPF, which

was based on the methodology described by Mansur *et al.* (30) In order to guarantee the reliability of the method, a commercially available sunscreen with a known protection factor (SPF = 30) was evaluated. The SPF values as determined by the *in vitro* spectrophotometric method are shown in Table VIII.

The result obtained for the commercially available sunscreen was $SPF_{\text{spectrophotometric}} = 10$, which does not match with the value labeled by the industry. From this information, a calculation was made to adjust the SPF obtained in the bemotrizinol-containing nanosystem whose approximate value was $SPF_{\text{NLCF}} = 10$.

The result after proper correction seems satisfactory, especially when taken into account that such a low concentration of organic filter (0.4% w/v of bemotrizinol) was used for the nanosystem development. On the other hand, the potential photoprotective effect of NLCF observed in Fig. 8 corroborates with that of the spectrophotometric SPF, where such effect is enhanced after incorporation of bemotrizinol into the nanoparticles.

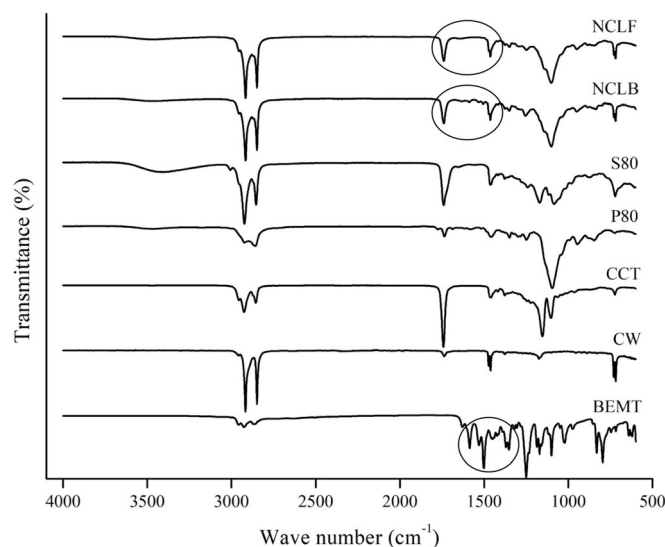


Fig. 7. FTIR spectra of the individual components as well as the NLCB and NLCF formulations

CONCLUSION

New sunscreen formulations based on nanostructured lipid carriers containing BEMT were developed and further characterized. The desired particle size was found by using an experimental design of the Box-Behnken type, which enabled a reduction in the time and costs of development process.

Besides obtaining particles smaller than 200 nm, the particles were found to be spherical and uniformly distributed. The crystallinity of the systems was evaluated through XRD, which evidenced the appearance of amorphous halos and reduction of crystallinity of CCT and BEMT when in NLCF.

The results of the *in vitro* photoprotective activity of the nanostructured lipid carriers containing BEMT were favorable and suggest a beneficial synergism between BEMT and carnauba wax-based nanostructured lipid carrier, promoting

an overall increase of the photoprotective activity which may result in a cost-effective economic impact.

In general, NLCF have shown to be a promising alternative for photoprotection, where it could be dispersed in different cosmetic forms including hydrogels. The increase in photoprotective activity without increasing the concentration of organic UV filter, in addition to the use of a more esthetically acceptable formulation with increased safety, makes NLC a promising alternative for new sunscreens and nanocosmetics.

In addition, to obtain nanostructured lipid carriers containing bemotrizinol, organic solvents are not used in any of the stages, in compliance with the first principle of green chemistry: preventing the formation of organic waste.

Studies to determine SPF *in vivo* are necessary in order to confirm the performance obtained in the *in vitro* study.

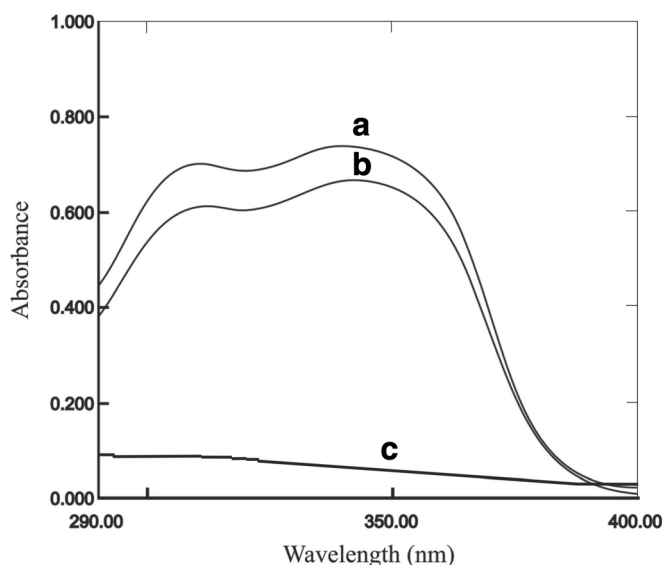


Fig. 8. Comparison of UV absorbance of NLCF (a), bemotrizinol solution (b), and NLCB (c)

Table VIII. *In vitro* Quantification of SPF Values (Mean \pm Standard Deviation; $n = 3$)

Formulation	Spectrophotometric SPF	Adjusted SPF
NLCF	3.43 \pm 0.08	11.04 \pm 0.08
NLCB	0.19 \pm 0.01	0.56 \pm 0.01
BEMT solution	1.50 \pm 0.04	4.78 \pm 0.04
Commercially available sunscreen	11.04 \pm 0.04	30.00

FUNDING

The study was financially supported by the PROPESQ-UEPB (4.03.00.005-400/2017-1), CNPq (453940/2014-5), and CAPES (Finance code 001).

COMPLIANCE WITH ETHICAL STANDARDS

Conflict of Interest The authors declare that they have no conflicts of interest.

REFERENCES

- Cestari TF, de Oliveira FB, Boza JC. Considerations on photoprotection and skin disorders. *Ann Dermatol Venereol.* 2012;139:135–43. [https://doi.org/10.1016/S0151-9638\(12\)70125-4](https://doi.org/10.1016/S0151-9638(12)70125-4).
- Young AR, Claveau J, Rossi AB. Ultraviolet radiation and the skin: photobiology and sunscreen photoprotection. *J Am Acad Dermatol.* 2017;76:100–9. <https://doi.org/10.1016/j.jaad.2016.09.038>.
- Sambandan DR, Ratner D. Sunscreens: an overview and update. *J Am Acad Dermatol.* 2011;64:748–58. <https://doi.org/10.1016/j.jaad.2010.01.005>.
- Watson M, Holman DM, Maguire-Eisen M. Ultraviolet radiation exposure and its impact on skin cancer risk. *Semin Oncol Nurs.* 2016;32:241–54. <https://doi.org/10.1016/j.soncn.2016.05.005>.
- Jansen R, Wang SQ, Burnett M, Osterwalder U, Lim HW. Photoprotection: part I. Photoprotection by naturally occurring, physical, and systemic agents. *J Am Acad Dermatol.* 2013;69:853.e1–853.e12. <https://doi.org/10.1016/j.jaad.2013.08.021>.
- Cozzi AC, Perugini P, Gourion-Arsiquaud S. Comparative behavior between sunscreens based on free or encapsulated UV filters in term of skin penetration, retention and photostability. *Eur J Pharm Sci.* 2018;121:309–18. <https://doi.org/10.1016/j.ejps.2018.06.001>.
- Heo S, Hwang HS, Jeong Y, Na K. Skin protection efficacy from UV irradiation and skin penetration property of polysaccharide-benzophenone conjugates as a sunscreen agent. *Carbohydr Polym.* 2018;195:534–41. <https://doi.org/10.1016/j.carbpol.2018.05.010>.
- Al-Jamal MS, Griffith JL, Lim HW. Photoprotection in ethnic skin. *Dermatol Sin.* 2014;32:217–24. <https://doi.org/10.1016/j.dsi.2014.09.001>.
- González S, Fernández-Lorente M, Gilaberte-Calzada Y. The latest on skin photoprotection. *Clin Dermatol.* 2008;26:614–26. <https://doi.org/10.1016/j.clindermatol.2007.09.010>.
- Morabito K, Shapley NC, Steeley KG, Tripathi A. Review of sunscreen and the emergence of non-conventional absorbers and their applications in ultraviolet protection. *Int J Cosmet Sci.* 2011;33:385–90. <https://doi.org/10.1111/j.1468-2494.2011.00654.x>.
- Chatelain E, Gabard B. Photostabilization of butyl methoxydibenzoylmethane (avobenzone) and ethylhexyl methoxycinnamate by bis-ethylhexyloxyphenol methoxyphenyl triazine (Tinosorb S), a new UV broadband filter. *Photochem Photobiol.* 2001;74:401–6.
- Cerqueira Coutinho C d S, dos Santos EP, Mansur CRE. Nanosystems in Photoprotection. *J Nanosci Nanotechnol.* 2015;15:9679–88. <https://doi.org/10.1166/jnn.2015.10512>.
- Gilbert E, Roussel L, Serre C, Sandouk R, Salmon D, Kirilov P, et al. Percutaneous absorption of benzophenone-3 loaded lipid nanoparticles and polymeric nanocapsules: a comparative study. *Int J Pharm.* 2016;504:48–58. <https://doi.org/10.1016/j.ijpharm.2016.03.018>.
- Alvarez-Román R, Barré G, Guya RH, Fessi H. Biodegradable polymer nanocapsules containing a sunscreen agent: preparation and photoprotection. *Eur J Pharm Biopharm.* 2001;52:191–5. [https://doi.org/10.1016/S0939-6411\(01\)00188-6](https://doi.org/10.1016/S0939-6411(01)00188-6).
- Villalobos-Hernández JR, Müller-Goymann CC. Novel nanoparticulate carrier system based on carnauba wax and decyl oleate for the dispersion of inorganic sunscreens in aqueous media. *Eur J Pharm Biopharm.* 2005;60:113–22. <https://doi.org/10.1016/j.ejpb.2004.11.002>.
- Nikolić S, Keck CM, Anselmi C, Müller RH. Skin photoprotection improvement: synergistic interaction between lipid nanoparticles and organic UV filters. *Int J Pharm.* 2011;414:276–84. <https://doi.org/10.1016/j.ijpharm.2011.05.010>.
- Manaia EB, Kaminski RCK, Soares CP, Meneau F, Pulcinelli SH, Santilli CV, et al. Liquid crystalline formulations containing modified surface TiO₂ nanoparticles obtained by sol-gel process. *J Sol-Gel Sci Technol.* 2012;63:251–7. <https://doi.org/10.1007/s10971-011-2673-7>.
- Puglia C, Damiani E, Offerta A, Rizza L, Tirendi GG, Tarico MS, et al. Evaluation of nanostructured lipid carriers (NLC) and nanoemulsions as carriers for UV-filters: characterization, in vitro penetration and photostability studies. *Eur J Pharm Sci.* 2014;51:211–7. <https://doi.org/10.1016/j.ejps.2013.09.023>.
- Baccarin T, Mitjans M, Ramos D, Lemos-Senna E, Vinardell MP. Photoprotection by Punica granatum seed oil nanoemulsion entrapping polyphenol-rich ethyl acetate fraction against UVB-induced DNA damage in human keratinocyte (HaCaT) cell line. *J Photochem Photobiol B Biol.* 2015;153:127–36. <https://doi.org/10.1016/j.jphotobiol.2015.09.005>.
- Gutiérrez-Hernández JM, Escalante A, Murillo-Vázquez RN, Delgado E, González FJ, Toriz G. Use of Agave tequilana-lignin and zinc oxide nanoparticles for skin photoprotection. *J Photochem Photobiol B Biol.* 2016;163:156–61. <https://doi.org/10.1016/j.jphotobiol.2016.08.027>.
- De Oliveira CA, Peres DDA, Graziola F, Chacra NAB, De Araújo GLB, Flórido AC, et al. Cutaneous biocompatible rutin-loaded gelatin-based nanoparticles increase the SPF of the association of UVA and UVB filters. *Eur J Pharm Sci.* 2016;81:1–9. <https://doi.org/10.1016/j.ejps.2015.09.016>.
- Lv X, Cong Z, Liu Z, Ma X, Xu M, Tian Y, et al. Improvement of the solubility, photostability, antioxidant activity and UVB photoprotection of trans-resveratrol by essential oil based microemulsions for topical application. *J Drug Deliv Sci Technol.* 2018;48:346–54. <https://doi.org/10.1016/j.jddst.2018.10.017>.
- Frizzo MS, Feuser PE, Berres PH, Ricci-Júnior E, Campos CEM, Costa C, et al. Simultaneous encapsulation of zinc oxide and octocrylene in poly (methyl methacrylate-co-styrene) nanoparticles obtained by miniemulsion polymerization for use in sunscreen formulations. *Colloids Surf A Physicochem Eng Asp.* 2019;561:39–46. <https://doi.org/10.1016/j.colsurfa.2018.10.062>.

24. Pardeike J, Hommoss A, Müller RH. Lipid nanoparticles (SLN, NLC) in cosmetic and pharmaceutical dermal products. *Int J Pharm.* 2009;366:170–84. <https://doi.org/10.1016/j.ijpharm.2008.10.003>.
25. Khurana S, Jain NK, Bedi PMS. Development and characterization of a novel controlled release drug delivery system based on nanostructured lipid carriers gel for meloxicam. *Life Sci.* 2013;93:763–72. <https://doi.org/10.1016/j.lfs.2013.09.027>.
26. Salminen H, Helgason T, Aulbach S, Kristinsson B, Kristbergsson K, Weiss J. Influence of co-surfactants on crystallization and stability of solid lipid nanoparticles. *J Colloid Interface Sci.* 2014;426:256–63. <https://doi.org/10.1016/j.jcis.2014.04.009>.
27. Jain P, Rahi P, Pandey V, Asati S, Soni V. Nanostructure lipid carriers: a modish contrivance to overcome the ultraviolet effects. *Egypt J Basic Appl Sci.* 2017;4:89–100. <https://doi.org/10.1016/j.ejbas.2017.02.001>.
28. Mitri K, Shegokar R, Gohla S, Anselmi C, Müller RH. Lipid nanocarriers for dermal delivery of lutein: preparation, characterization, stability and performance. *Int J Pharm.* 2011;414:267–75. <https://doi.org/10.1016/j.ijpharm.2011.05.008>.
29. Abdel-Salam FS, Ammar HO, Elkheshen SA, Mahmoud AA. Anti-inflammatory sunscreen nanostructured lipid carrier formulations. *J Drug Deliv Sci Technol.* 2017;37:13–9. <https://doi.org/10.1016/j.jddst.2016.10.014>.
30. Sala M, Diab R, Elaissari A, Fessi H. Lipid nanocarriers as skin drug delivery systems: properties, mechanisms of skin interactions and medical applications. *Int J Pharm.* 2018;535:1–17. <https://doi.org/10.1016/j.ijpharm.2017.10.046>.
31. Mansur JS, Breder MNR, Mansur MCD, Azulay RD. Determinação do fator de proteção solar por espectrofotometria. *An Bras Dermatol.* 1986;61:121–4.
32. Sayre RM, Agin PP, Levee GJ, Marlowe E. A comparison of in vivo and in vitro testing of sunscreens formulas. *Photochem Photobiol.* 1979;29:559–66.
33. Thapa C, Ahad A, Aqil M, Imam SS, Sultana Y. Formulation and optimization of nanostructured lipid carriers to enhance oral bioavailability of telmisartan using Box–Behnken design. *J Drug Deliv Sci Technol.* 2018;44:431–9. <https://doi.org/10.1016/j.jddst.2018.02.003>.
34. Aditya NP, Macedo AS, Doktorovova S, Souto EB, Kim S, Chang PS, et al. Development and evaluation of lipid nanocarriers for quercetin delivery: a comparative study of solid lipid nanoparticles (SLN), nanostructured lipid carriers (NLC), and lipid nanoemulsions (LNE). *LWT Food Sci Technol.* 2014;59:115–21. <https://doi.org/10.1016/j.lwt.2014.04.058>.
35. Gaba B, Fazil M, Khan S, Ali A, Baboota S, Ali J. Nanostructured lipid carrier system for topical delivery of terbinafine hydrochloride. *Bull Fac Pharm, Cairo Univ.* 2015;53:147–59. <https://doi.org/10.1016/j.bfopcu.2015.10.001>.
36. Sato MR, Oshiro Junior JA, Machado RTA, de Souza PC, Campos DL, Pavan FR, et al. Nanostructured lipid carriers for incorporation of copper (II) complexes to be used against *Mycobacterium tuberculosis*. *Drug Des Devel Ther.* 2017;11:909–21. <https://doi.org/10.2147/DDDT.S127048>.
37. Junyaprasert VB, Teeranachaideekul V, Souto EB, Boonme P, Müller RH. Q10-loaded NLC versus nanoemulsions: stability, rheology and in vitro skin permeation. *Int J Pharm.* 2009;377:207–14. <https://doi.org/10.1016/j.ijpharm.2009.05.020>.
38. Kovacevic A, Savic S, Vuleta G, Müller RH, Keck CM. Polyhydroxy surfactants for the formulation of lipid nanoparticles (SLN and NLC): effects on size, physical stability and particle matrix structure. *Int J Pharm.* 2011;406:163–72. <https://doi.org/10.1016/j.ijpharm.2010.12.036>.
39. Wissing SA, Müller RH. A novel sunscreen system based on tocopherol acetate incorporated into solid lipid nanoparticles. *Int J Cosmet Sci.* 2001;23:233–43. <https://doi.org/10.1046/j.1467-2494.2001.00087.x>.
40. Wang W, Chen L, Huang X, Shao A. Preparation and characterization of minoxidil loaded nanostructured lipid carriers. *AAPS PharmSciTech.* 2017;18:509–16. <https://doi.org/10.1208/s12249-016-0519-x>.
41. Rapalli VK, Kaul V, Waghule T, Gorantla S, Sharma S. Curcumin loaded nanostructured lipid carriers for enhanced skin retained topical delivery: optimization, scale-up, in-vitro characterization and assessment of ex-vivo skin deposition. *Eur J Pharm Sci.* 2020;152:105438. <https://doi.org/10.1016/j.ejps.2020.105438>.
42. Abila MJ, Banga AK. Formulation of tocopherol nanocarriers and in vitro delivery into human skin. *Int J Cosmet Sci.* 2014;36:239–46. <https://doi.org/10.1111/ics.12119>.
43. Pinto F, Fonseca LP, Souza S, Oliva A, de Barros DP. Topical distribution and efficiency of nanostructured lipid carriers on a 3D reconstructed human epidermis model. *J Drug Deliv Sci Technol.* 2020;101616:101616. <https://doi.org/10.1016/j.jddst.2020.101616>.
44. Haque T, Crowther JM, Lane ME, Moore DJ. Chemical ultraviolet absorbers topically applied in a skin barrier mimetic formulation remain in the outer stratum corneum of porcine skin. *Int J Pharm.* 2016;510:250–4. <https://doi.org/10.1016/j.ijpharm.2016.06.041>.
45. Castelli F, Puglia C, Sarpietro MG, Rizza L, Bonina F. Characterization of indomethacin-loaded lipid nanoparticles by differential scanning calorimetry. *Int J Pharm.* 2005;304:231–8. <https://doi.org/10.1016/j.ijpharm.2005.08.011>.
46. Uprit S, Kumar Sahu R, Roy A, Pare A. Preparation and characterization of minoxidil loaded nanostructured lipid carrier gel for effective treatment of alopecia. *Saudi Pharm J.* 2013;21:379–85. <https://doi.org/10.1016/j.sjps.2012.11.005>.
47. Freitas CAS, Vieira ÍGP, Sousa PHM, Muniz CR, Gonzaga MLDC, Guedes MIF. Carnauba wax p-methoxycinnamic diesters: characterisation, antioxidant activity and simulated gastrointestinal digestion followed by in vitro bioaccessibility. *Food Chem.* 2016;196:1293–300. <https://doi.org/10.1016/j.foodchem.2015.10.101>.
48. Pradhan M, Singh D, Murthy SN, Singh MR. Design, characterization and skin permeating potential of fluocinonide acetone loaded nanostructured lipid carriers for topical treatment of psoriasis. *Steroids.* 2015;101:56–63. <https://doi.org/10.1016/j.steroids.2015.05.012>.
49. Agrawal Y, Petkar KC, Sawant KK. Development, evaluation and clinical studies of acitretin loaded nanostructured lipid carriers for topical treatment of psoriasis. *Int J Pharm.* 2010;401:93–102. <https://doi.org/10.1016/j.ijpharm.2010.09.007>.
50. Sanad RA, AbdelMalak NS, Badawi AA. Formulation of a novel oxybenzone-loaded nanostructured lipid carriers (NLCs). *AAPS PharmSciTech.* 2010;11:1684–94. <https://doi.org/10.1208/s12249-010-9553-2>.
51. Imran M, Iqbal MK, Imtiyaz K, Saleem S, Mittal S, Rizvi MMA, et al. Topical nanostructured lipid carrier gel of quercetin and resveratrol: formulation, optimization, in vitro and ex vivo study for the treatment of skin cancer. *Int J Pharm.* 2020;119705. <https://doi.org/10.1016/j.ijpharm.2020.119705>.
52. Li B, Ge ZQ. Nanostructured lipid carriers improve skin permeation and chemical stability of idebenone. *AAPS PharmSciTech.* 2012;13:276–83. <https://doi.org/10.1208/s12249-011-9746-3>.
53. Tran TH, Ramasamy T, Truong DH, Choi HG, Yong CS, Kim JO. Preparation and characterization of fenofibrate-loaded nanostructured lipid carriers for oral bioavailability enhancement. *AAPS PharmSciTech.* 2014;15:1509–15. <https://doi.org/10.1208/s12249-014-0175-y>.
54. Dan N. Compound release from nanostructured lipid carriers (NLCs). *J Food Eng.* 2016;171:37–43. <https://doi.org/10.1016/j.jfoodeng.2015.10.005>.
55. Khosa A, Reddi S, Saha RN. Nanostructured lipid carriers for site-specific drug delivery. *Biomed Pharmacother.* 2018;103:598–613. <https://doi.org/10.1016/j.biopha.2018.04.055>.
56. Santiago RR, Silva KGDH, Santos ND, Genre J, Oliveira LVF, Silva AL, et al. Nanostructured lipid carriers containing amphotericin B: development, in vitro release assay, and storage stability. *J Drug Deliv Sci Technol.* 2018;48:372–82. <https://doi.org/10.1016/j.jddst.2018.10.003>.
57. Motawea A, Abd El-Gawad HAEG, Borg T, Motawea M, Tarshoby M. The impact of topical phenytoin loaded nanostructured lipid carriers in diabetic foot ulceration. *Foot.* 2019;40:14–21. <https://doi.org/10.1016/j.foot.2019.03.007>.
58. Espinosa-Olivares MA, Delgado-Buenrostro NL, Chirino YI, Trejo-Marquez MA, Pascual-Bustamante S, Gnem-Rondero A. Nanostructured lipid carriers loaded with curcuminoids:

- physicochemical characterization, in vitro release, ex vivo skin penetration, stability and antioxidant activity. *Eur J Pharm Sci.* 2020;105533. <https://doi.org/10.1016/j.ejps.2020.105533>.
59. Müller RH, Radtke M, Wissing SA. Solid lipid nanoparticles (SLN) and nanostructured lipid carriers (NLC) in cosmetic and dermatological preparations. *Adv Drug Deliv Rev.* 2002;54:S131–55. [https://doi.org/10.1016/S0169-409X\(02\)00118-7](https://doi.org/10.1016/S0169-409X(02)00118-7).
60. Prado AH, Araújo VHS, Eloy JO, Fonseca-Santos B, Pereira-da-Silva MA, Peccinini RG, et al. Synthesis and characterization of nanostructured lipid nanocarriers for enhanced sun protection factor of Octyl p-methoxycinnamate. *AAPS PharmSciTech.* 2020;21:125. <https://doi.org/10.1208/s12249-019-1547-0>.
61. Tahir N, Madni A, Balasubramanian V, Rehman M, Correia A, Kashif PM, et al. Development and optimization of methotrexate-loaded lipid-polymer hybrid nanoparticles for controlled drug delivery applications. *Int J Pharm.* 2017;533:156–68. <https://doi.org/10.1016/j.ijpharm.2017.09.061>.
62. Villalobos-Hernández JR, Müller-Goymann CC. Sun protection enhancement of titanium dioxide crystals by the use of carnauba wax nanoparticles: the synergistic interaction between organic and inorganic sunscreens at nanoscale. *Int J Pharm.* 2006;322:161–70. <https://doi.org/10.1016/j.ijpharm.2006.05.037>.

Publisher's Note Springer Nature remains neutral with regard to jurisdictional claims in published maps and institutional affiliations.